Journal of
Marine Science and Engineering

MDPI

Article

A Study on Crack Initiation and Propagation of Welded Joints under Explosive Load

Penglong Ding [1,2], Xuhui Gong [2,3], Lei Sun [2,3], Jiajia Niu [2], Youjing Zhang [2,3,*] and Lianyong Xu [1]

[1] School of Materials Science and Engineering, Tianjin University, Tianjin 300350, China; dingpenglong@126.com (P.D.)
[2] Luoyang Ship Material Research Institute, Luoyang 471000, China
[3] National Key Laboratory of Marine Corrosion and Protection, Luoyang 471000, China
* Correspondence: zhangyoujing1988@126.com

Abstract: Welded joints in naval ship hull structures are weak areas under explosive load, but there are relatively few studies investigating the failure characteristics of welded joints through dynamic fracture and explosion tests. In order to explore and predict the failure characteristics of welded joints under explosive load, instrumented Charpy impact tests, explosion tests, and numerical simulations were carried out. The dynamic fracture toughness of ultra-high strength ship hull structural steel welded joints was obtained, and the dynamic stress intensity factors, together with the correlation between stress wave and crack propagation at different positions, were acquired. The results showed that the stress state at the crack tip of a Charpy impact specimen was consistent with that of a welded joint under explosive loads, and the crack initiated when the dynamic stress intensity factor exceeded the dynamic fracture toughness. The results indicated that the dynamic fracture toughness obtained by instrumented Charpy impact tests could be used to predict the crack initiation characteristics of welded structures under explosive load, and the stress wave at the crack tip was basically perpendicular to the crack propagation surface and promoted the rapid propagation of cracks.

Keywords: explosive load; butt joint; dynamic fracture toughness; crack initiation and propagation

check for updates

Citation: Ding, P.; Gong, X.; Sun, L.; Niu, J.; Zhang, Y.; Xu, L. A Study on Crack Initiation and Propagation of Welded Joints under Explosive Load. *J. Mar. Sci. Eng.* **2024**, *12*, 927. https://doi.org/10.3390/jmse12060927

Academic Editor: Joško Parunov

Received: 9 May 2024
Revised: 24 May 2024
Accepted: 28 May 2024
Published: 31 May 2024

Copyright: © 2024 by the authors. Licensee MDPI, Basel, Switzerland. This article is an open access article distributed under the terms and conditions of the Creative Commons Attribution (CC BY) license (https://creativecommons.org/licenses/by/4.0/).

1. Introduction

With the rapid development of ultra-high-speed attack weapons, stealth anti-ship missiles, and new torpedoes, the safety of naval ships has been seriously threatened. Under the action of explosive shock waves, the ship structure will undergo extensive damage and fracture, resulting in the loss of combat effectiveness and even the direct sinking of the ship. How to improve the anti-explosion performance of ship structure and enhance the level of survival in the battlefield is a major issue that must be addressed by the armed forces of all countries [1–4]. Naval ship structures are mainly fabricated by welding of high-strength steel [5]. Due to uneven heating and cooling caused by the welding process, weld flaws, locally embrittled regions, and welding residual stress are inevitable. On the other hand, weld reinforcement generates geometric discontinuities and stress concentration in the toe region. These lead to the complexity of the failure behavior of the welded joint under high-speed dynamic loads, making it a weak area of the entire ship's anti-explosion performance [6]. Therefore, it is necessary to investigate the failure behavior and mechanism of the welding joint under explosive loads.

The failure behavior of welded joints under explosive loads involves the calculation of blasting loads, structural dynamic response, and dynamic crack initiation and propagation, which exhibit high structural nonlinearity and material nonlinearity. Some scholars have conducted studies on crack problems under explosive loads. Chuanjin Pu [7] used Autodyn software 18.0 to study the crack propagation of plexiglass (PMMA) materials under explosive loads. By introducing a tensile fracture softening failure model, he obtained the

crack propagation characteristics under single-hole and double-hole drilling conditions. Cheng Shufan [8] analyzed the crack propagation and material damage distribution of rock masses under explosive loads using the HJC model and the virtual-damage crack model of the cleavage cohesion element. Li Qing [9] and Yang Renshu [10], among others, explored the interaction between cracks and stress waves under explosive loads using a transmission-type explosive dynamic caustics optical test system. The results showed that stress waves have a significant impact on the dynamic characteristics of crack tips. Wan Duanying [11] adopted a test system composed of an oscilloscope, an ultra-dynamic strain gauge, and a crack propagation meter to monitor the propagation speed and distance of the main crack. Although these studies directly considered explosive loads, they mainly focused on brittle materials such as rocks and plexiglass. However, ship structural steel has a high level of toughness and plasticity, and its failure behavior differs from brittle materials.

Dynamic fracture toughness is an important parameter for evaluating crack initiation and propagation under dynamic loads, as well as a threshold parameter characterizing metal material failure due to fracture. In terms of this problem, Zou Guangping [12] improved the split Hopkinson tension bar and used finite element simulations to reconstruct the dynamic fracture tests of compact tension specimens. He explored the influence of clamping devices on the test results and obtained the dynamic fracture toughness of aluminum alloy materials by calculating the dynamic J-integral and converting it based on the relationship between linear elastic fracture mechanics J and stress intensity factor K. Wu Yungang [13] used ABAQUS to numerically simulate the dynamic fracture experiment of the Hopkinson compression bar and obtained the dynamic stress intensity factor curve at the crack tip using the node displacement method. Combined with the crack initiation time in the dynamic fracture test specimen, he obtained the dynamic fracture stress intensity factor of the pipeline weldment. Pan Jianhua [14] conducted a shock wave impact test and numerical simulation to investigate the dynamic fracture behavior of S304 austenitic stainless steel and weld joints containing prefabricated cracks. Wang Jiabin [15] and Yi Haijiao [16] also conducted dynamic three-point bending tests to study the dynamic fracture toughness of materials with typical high strength and toughness, such as X80 steel and GH4169 nickel-based alloys, and further studies were conducted using advanced fracture simulation methods such as the virtual crack closure technique. Some institutes also conducted research on the response of hull plate-girder structures under explosive loading, but they did not consider the effect of welds [17–21]. These studies have been conducted from multiple dimensions of theory, experimentation, and virtual simulation, and relevant parameters characterizing the dynamic crack initiation and propagation of metal materials are acquired. However, current research has not directly coupled the explosive load with crack initiation or propagation behavior, and it is unclear whether these characterization parameters are directly applicable to explosive loads.

Based on the above analysis, current studies directly considering crack behavior under explosive loads mainly focus on brittle materials, while studies on the dynamic fracture and propagation of metallic materials have not directly considered explosive loads. Research on the failure characteristics of ship structural steel welded joints under explosive loads is also insufficient. To solve this problem, it is necessary to consider both dynamic fracture toughness and explosive loads simultaneously. This study initially evaluates the dynamic fracture toughness of weld joints in ship hull structural steel using instrumented Charpy impact tests. Subsequently, the strain and stress data of the Charpy impact specimen are acquired through numerical simulations. Following this, the response and failure characteristics of butt joints are examined through explosion experiments and simulations. Then, it investigates the suitability of dynamic fracture toughness in characterizing butt joint failures. Finally, the influence of stress waves on crack propagation is explored.

2. Materials and Methods

2.1. Dynamic Fracture Toughness Measurement

Currently, the dynamic fracture test under pendulum impact conditions (the instrumented impact test) using three-point bending specimens still holds a dominant position in the field. Its general loading rate ranges from 10^3 MPa·m$^{0.5}$/s to 10^5 MPa·m$^{0.5}$/s, making it a simple, convenient, and cost-effective method [22–24]. Studying the dynamic fracture behavior of metallic materials using this method is significant at the current stage. In this study, using the standard ASTM E23 [25], Charpy impact specimens had dimensions of thickness B = 10 mm, width W = 10 mm, length L = 55 mm, span S = 40 mm, with a notch angle of 45 degrees and a notch length of 2 mm. A fatigue crack was prefabricated by wire cutting to a certain depth.

For ultra-high-strength ship hull structural steel butt joints, the instrumented Charpy impact tests were conducted on metal specimens, weld metal specimens, and heat-affected zone (HAZ) specimens with prefabricated fatigue notches. The notch location for the specimens is shown in Figure 1. The dynamic fracture toughness values of the specimens were determined based on load–displacement curves (Figure 2). For linear elastic fracture, the dynamic fracture toughness can be calculated using Formulas (1)–(3) [26,27]. The chemical composition of the ship hull steel is presented in Table 1.

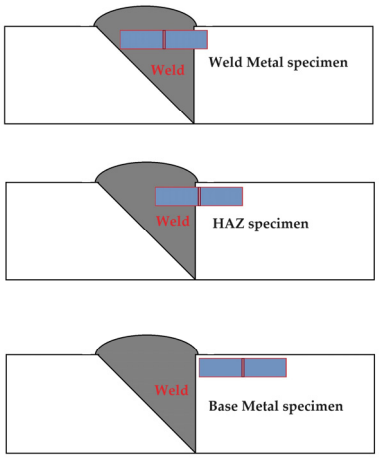

Figure 1. Notch location of test specimens.

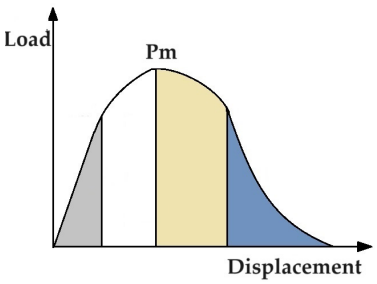

Figure 2. The typical load–displacement curve of the instrumented impact test.

Table 1. Chemical composition of the ship hull steel (wt%).

Element	C	Si	Mn	S	P	Ni	Cr	Mo	V
Proportion	0.09	0.5	0.2	0.001	0.001	3.1	0.34	1.1	0.06

The linear elastic fracture toughness calculation formula is as follows:

$$K_{Id} = \frac{P_m \cdot S}{B \cdot W^{1.5}} \cdot f\left(\frac{a}{W}\right) \quad (1)$$

$$f\left(\frac{a}{W}\right) = \frac{3\left(\frac{a}{W}\right)^{1/2}\left(1.99 - \left(\frac{a}{W}\right)1 - \left(\frac{a}{W}\right)\right) \times \left(2.15 - 3.93\frac{a}{W} + 2.7\frac{a^2}{W^2}\right)}{2\left(1 + \frac{2a}{W}\right)\left(1 - \frac{a}{W}\right)^{3/2}} \quad (2)$$

$$\dot{K}_{Id} = \frac{K_{Id}}{t_m} \quad (3)$$

In Figure 2 and Formulas (1)–(3), K_{Id} represents dynamic fracture toughness, P_m represents the maximum impact load, S represents the span length, B represents the specimen thickness, a represents the notch depth, W represents the specimen width, $\dot{K}_{Id}$ is the dynamic fracture toughness rate, and t_m represents the time corresponding to the maximum force.

To obtain the strain rate and stress state information during the instrumented impact test, numerical simulations were carried out using Ls-dyna. The finite element model for the Charpy impact test is shown in Figure 3, which includes the impact specimen, supports, and pendulum. The supports and pendulum were set as rigid bodies, maintaining frictional contact with the specimen. By applying the experimentally obtained displacement–time curve (Figure 4) to the pendulum, the impact process was simulated.

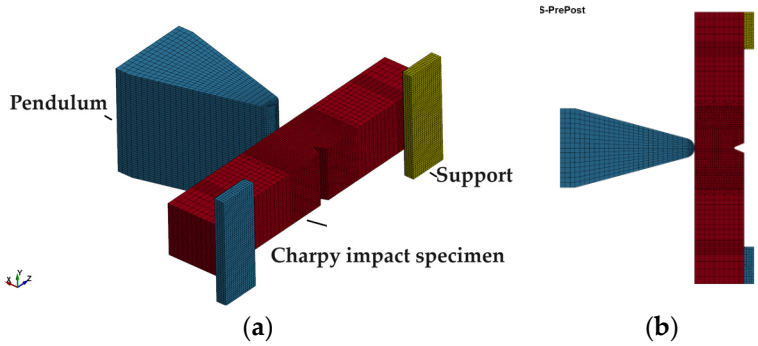

Figure 3. FEM for Charpy impact tests: (**a**) isometric view; (**b**) top view.

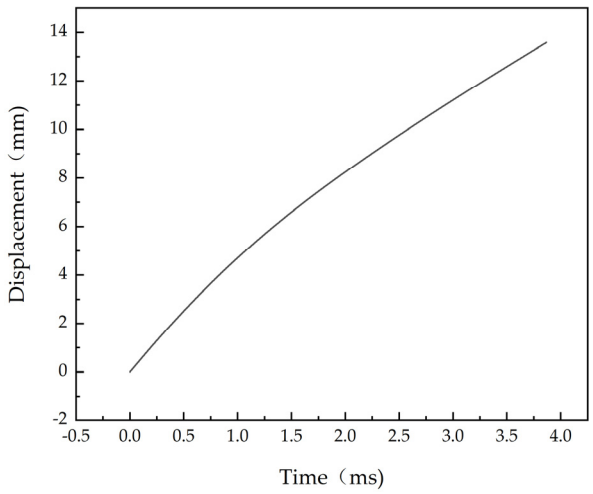

Figure 4. Displacement history curve from Charpy impact test.

2.2. Explosion Bulge Test on Butt Joint Plate

To investigate the characteristics of crack initiation and propagation in welded plates under explosive loads, and to verify the feasibility and accuracy of numerical simulations for explosions, two explosion bulge tests on butt joint plates were conducted referring to relevant US military standards [28]. The test results included the deformation and failure of the butt joint plates.

The butt joint plates had dimensions of 640 mm × 640 mm × 40 mm, and the explosion test diagram is shown in Figure 5. The explosion test system consisted of explosives (TNT),

the test plate, and a backup plate. The test plate was freely placed on the backup plate, and the TNT explosive was suspended directly above the test plate. The thickness reduction rate of the plate was determined by measuring the thickness changes at specific measurement points, as shown in Figure 5b and Formula (4). The TNT equivalent weight in the explosion test was 48 kg, with a detonation distance of 400 mm.

$$r = \frac{T_0 - T}{T_0} \tag{4}$$

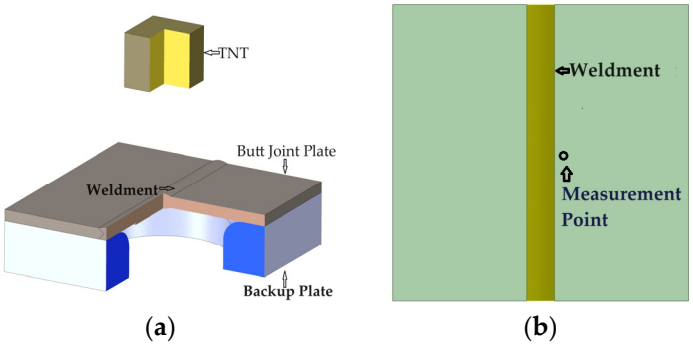

Figure 5. The arrangement of the explosion test: (**a**) section view of explosion test system; (**b**) thickness reduction rate measuring point.

In Formula (4), r represents the thickness reduction rate, T represents the thickness of the plate after explosion, and T_0 represents the thickness of the plate before the explosion.

2.3. Explosion Simulation of the Butt Joint Plate

An explosion test is the most direct and effective method to evaluate the blast resistance of structures, providing the most authentic results. However, explosion tests consume significant resources, pose safety risks, and have difficulties in capturing the evolution details of structural explosion damage. Meanwhile, numerical simulation methods have been widely used in studies on explosion, which not only saves a significant amount of time and material costs but also allows for the recreation of the explosion process, enabling us to obtain the structural motion response and failure mechanism under explosive loads. The response and failure behavior of structures under explosive loads are highly nonlinear, involving the generation, transmission, and coupling of explosion shock waves with the structure, as well as the crack initiation, propagation, and failure of materials. This is an extremely complex process that places high demands on the reliability of numerical simulations. Therefore, it is necessary to conduct benchmarking studies through explosion tests and numerical simulations to verify the accuracy of numerical methods, enabling further research to provide support for ship design.

The explicit dynamics finite element software Ls-Dyna 13 was used. The finite element model for the explosion bulge test simulation included the butt joint plate and the backup plate. The specimen dimensions were kept consistent with the experimental conditions, with the butt joint plate measuring 640 mm × 640 mm × 40 mm. The butt joint plate was divided into the base material, heat-affected zone, and weld zone. Due to the symmetry of the model, a half model was used for simulation to improve computational efficiency. Hexahedral elements were employed, with fine meshes of 1–2 mm in the bulging area and weld zone, and larger meshes in the remaining parts, totaling approximately 500,000 elements. The backup plate only provided support and was not specifically calculated, so it was set as a rigid body with fixed constraints applied. The backup plate and test plate had free contact with a friction coefficient of 0.1. The Johnson-Cook (J-C) constitutive model

was chosen, including the strength and failure parameters. The cumulative damage can be calculated by the J-C failure model, as shown in Formulas (5) and (6).

$$\varepsilon_f = [D_1 + D_2 exp D_3 \sigma^*]\left[1 + D_4 ln\dot{\varepsilon}^*\right][1 + D_5 T^*] \quad (5)$$

$$D = \sum \frac{\Delta\varepsilon}{\varepsilon_f} \quad (6)$$

In Formula (5), ε_f represents the failure strain, σ^* represents the stress triaxiality, $\dot{\varepsilon}^*$ represents the strain rate, T^* represents the relative temperature, and D_1~D_5 represent the material constant. In Formula (6), $\Delta\varepsilon$ represents the equivalent plastic strain in an integral cycle, and D represents the cumulative damage. When D = 1, the elements satisfy the failure criteria and are deleted.

The parameters of the J-C failure model are listed in Table 2.

Table 2. Parameters of J-C failure model.

D_1	D_2	D_3	D_4	D_5
0.31	1.21	−2.2	−0.03	1.02

The explosion load was applied by the ''load-blast'' command in Ls-dyna, with the TNT equivalent weight and the detonation distance of 400 mm kept the same as the tests. The finite element mesh model of the butt-welded plate is shown in Figure 6.

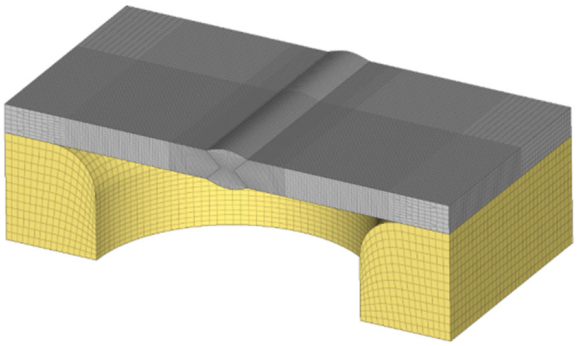

Figure 6. FEM of butt joint plate.

3. Results

3.1. Dynamic Fracture Toughness

A typical fracture surface photograph after the instrumented Charpy impact tests is shown in Figure 7. The dynamic fracture toughness values are presented in Table 3.

Figure 7. Specimens for dynamic fracture toughness.

Table 3. Dynamic fracture toughness.

Sampling Position	K_{Id}/MPa·m$^{0.5}$
Base Metal	265
HAZ	232
Weld Metal	196

The results in Table 3 show that the dynamic fracture toughness of the base metal is the highest, which reaches 265 MPa·m$^{0.5}$, while the weld metal has the lowest value 196 MPa·m$^{0.5}$, and the value of HAZ is 232 MPa·m$^{0.5}$.

The strain rate and stress triaxiality information of the specimen during the impact process obtained from the simulation are shown in Figures 8 and 9.

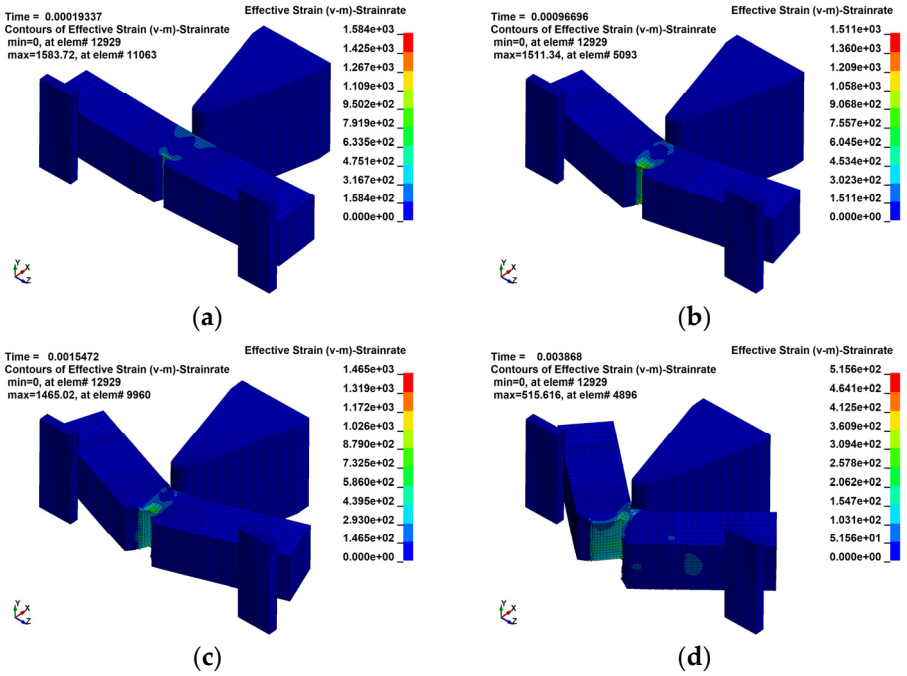

Figure 8. Strain rate distribution of Charpy impact test: (**a**–**d**) strain rate at different times.

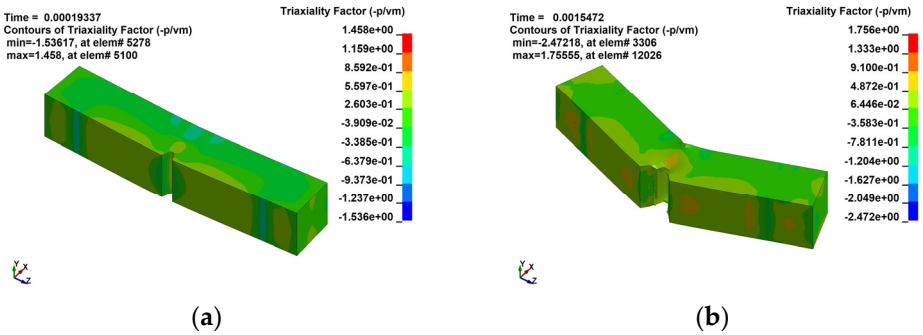

Figure 9. *Cont.*

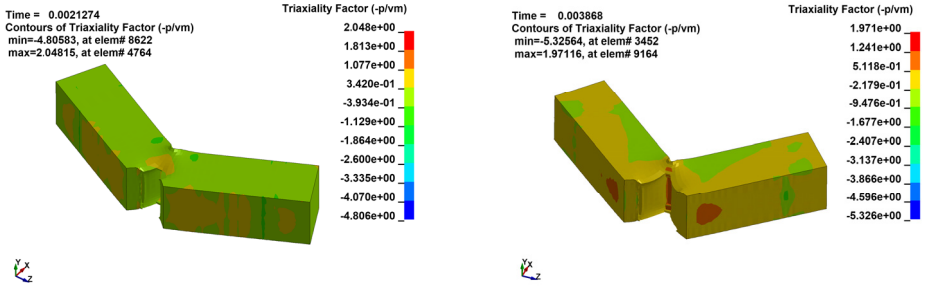

(**c**) (**d**)

Figure 9. Stress triaxiality distribution Charpy impact test: (**a**–**d**) stress triaxiality at different times.

A comparison of the extracted force-displacement curve of the pendulum with the experimental values is shown in Figure 10. A comparison of the impact energy obtained from the experiment with the simulated values is shown in Figure 11.

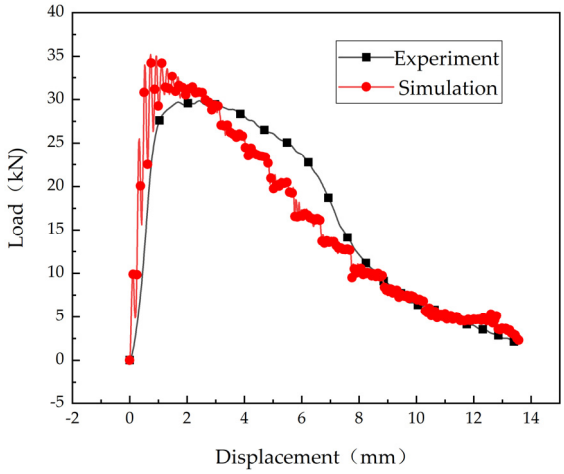

Figure 10. Load-displacement curve comparison.

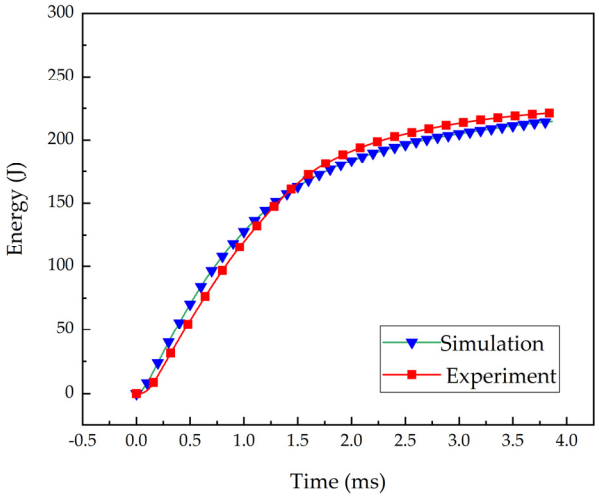

Figure 11. Impact energy curve comparison.

According to Figure 8, when the pendulum is in contact with the specimen, the specimen is deformed, and the strain rate at the notch is the highest and varies with time. As the pendulum displacement increases, the Charpy impact specimen cracks from the notch, and the crack propagates along the thickness direction, it is evident that the strain rate of the impact specimen is approximately 1500/s at the instant of crack initiation

(Figure 8a). From the stress triaxiality contour of the impact specimen (Figure 9), it is observed that the stress triaxiality at the notch of the impact specimen ranges from 0.5 to 2 at the time of failure, which indicates that the specimen undergoes tensile failure. As seen in Figure 10, the force–displacement curve obtained from the simulation is more consistent with the experimental curve in the front and rear sections, and the middle section is lower than the experimental values. In Figure 11, the impact energy curve obtained from the simulation basically overlaps with the experimental curve. Based on the comparison of the load–displacement curve and the energy–time curve in the figure, it can be seen that the simulation provides relatively accurate outcomes.

3.2. Explosion Bulge Test Results

After the explosion bulge tests, images were taken from the failure morphology of the butt joint plates, which are shown in Figure 12. The thickness reduction rate is shown in Table 4.

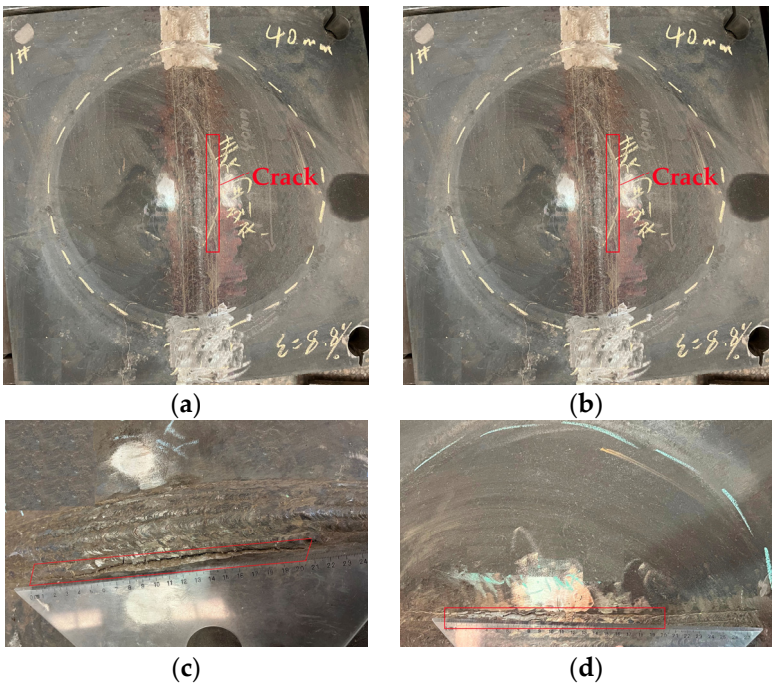

(**a**) (**b**)

(**c**) (**d**)

Figure 12. Butt joint plates after explosion test: (**a**) explosive bulge test plate 1; (**b**) explosive bulge test plate 2; (**c**) crack length of test plate 1; (**d**) crack length of test plate 2.

Table 4. Explosion test results.

Test Plates	Thickness Reduction Rate/%	Crack Length/mm
1	8.8	198
2	8.2	203

As seen in Figure 12, under an explosive load, the center of the specimen exhibits a "straw hat" shape protrusion, indicating that significant plastic deformation occurs. According to the thickness reduction rate statistics in Table 4, the average thickness reduction rate is 8.5%. Although there is no overall failure, a crack (marked the cracks in the figure with red boxes) of approximately 200 mm occurs along the weld toe in the central region of the plate.

3.3. Explosion Simulation Results

The calculated deformation, equivalent stress, plastic strain, strain rate, and cumulative damage of the butt joint plate are presented in Figure 13. The crack length of the butt

joint plate is shown in Figure 14. The thickness reduction rate history curve is presented in Figure 15. A comparison of the thickness reduction rate obtained from the simulation with the experimental values is presented in Table 5.

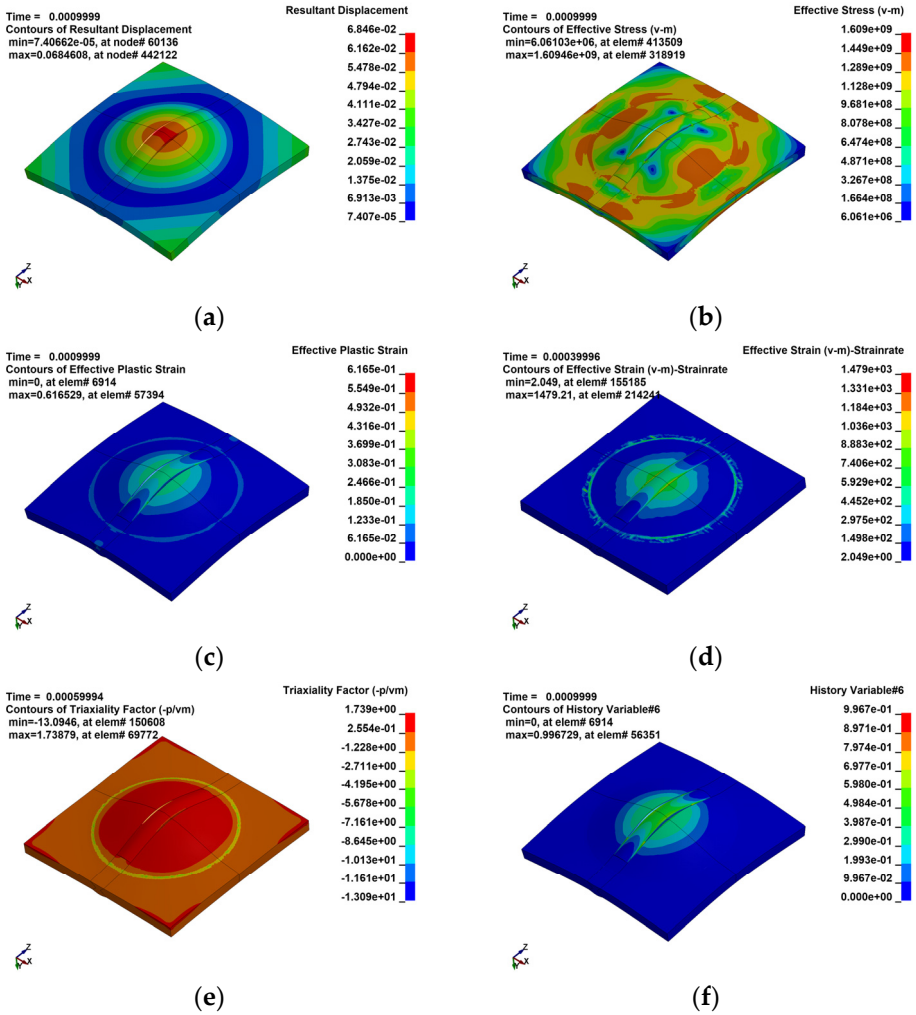

Figure 13. Simulation results of butt joint plate: (**a**) deformation; (**b**) equivalent stress; (**c**) plastic strain; (**d**) plastic strain rate; (**e**) stress triaxiality; (**f**) cumulative damage.

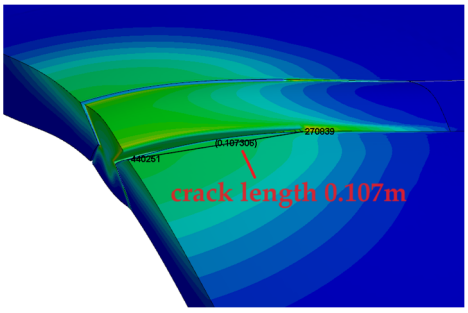

Figure 14. Crack length on butt joint plate (half-symmetry model).

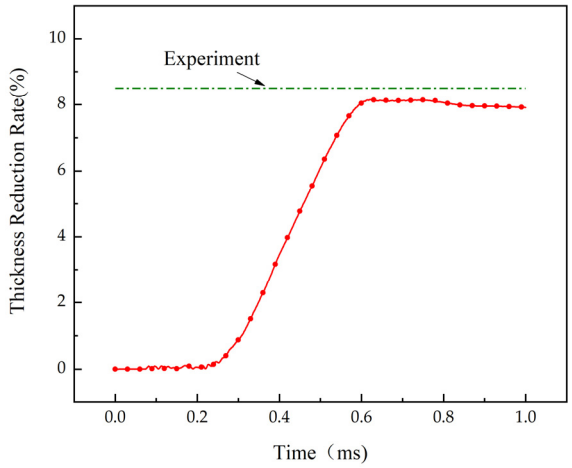

Figure 15. Thickness reduction rate history curve.

Table 5. Comparison of thickness reduction rate between experiment and simulation.

Method	Thickness Reduction Rate/%	Error/%
Experiment	8.5	7
Simulation	7.9	

As seen in Figure 13, the deformation pattern of the butt joint plate is characterized by a bulge in the middle, resembling a "straw hat" shape, with the maximum deformation occurring in the weld zone at the center of the plate, which is in alignment with the test results. From the stress contour plot, it can be observed that the maximum stress occurs in the fusion line region. The maximum plastic strain also occurs in the fusion line region. The stress triaxiality at the weld toe ranges from 0.5 to 1.8, and the strain rate is around 1479/s, similar to that observed at the notch of an impact specimen, indicating that the measurement of dynamic fracture toughness through instrumented impact testing can be used to characterize the material properties under explosive loading.

According to Figure 14, it can be seen that the crack initiates in the weld toe region at the center of the plate and propagates along the fusion line. The crack length is approximately 210 mm, which is basically consistent with the experimental measurement value of 200 mm.

As shown in Figure 15, the thickness reduction rate–time curve on the measurement point was compared with the experimental average value. The thickness reduction rate increases rapidly and then stabilizes, indicating that the plastic deformation of the structure ends in a short time. The stabilized thickness reduction rate of the butt joint plate obtained from the simulation is 7.9%, with a 7% error compared to the experimental value, indicating a high degree of credibility for the explosion simulation.

The numerical simulation model was validated through multiple aspects, including deformation morphology, crack length, and thickness reduction rate, demonstrating the high reliability of the explosion simulation. Afterward, dynamic fracture studies were conducted based on the validated finite element model.

4. Discussion

4.1. Discussion on Dynamic Crack Initiation under Explosion Load

In static conditions, the criterion for the initiation of opening-mode cracks is generally expressed as $K_I \geq K_{Ic}$ where K_I is the static stress intensity factor, and K_{Ic} is the static fracture toughness. Under dynamic loading, the stress intensity factor at the crack tip is a function of time, and the criterion for crack initiation is similar to the static case, expressed as $K_I(t) \geq K_{Id}$, where $K_I(t)$ is the dynamic stress intensity factor, which is time-dependent; K_{Id} is the dynamic fracture toughness, which is rate-dependent. Generally speaking, in the

above-mentioned crack initiation criterion under dynamic loading, the dynamic fracture toughness K_{Id} needs to be determined through experiments, while the dynamic stress intensity factor $K_I(t)$ needs to be determined through a complete dynamic analysis.

Dynamic problems are complex and involve the interaction between the crack tip and stress waves; therefore, only some simple ideal models have analytical solutions. In recent years, dynamic numerical analysis methods have expanded the scope of problem-solving, and the finite element method is the most commonly used, which is further divided into node displacement methods, J-integral methods, and virtual crack closure techniques. Currently, explicit dynamic algorithms cannot directly calculate the K value at the crack tip, but the K value can be indirectly obtained by calculating the J-integral. Rice has proven that the J-integral is the elastic strain energy release rate G_1, thus establishing the relationship between the J-integral, G_1, and the stress intensity factor K_I.

$$J = G_1 = \frac{K_I^2}{E_1} \tag{7}$$

where $E_1 = \begin{cases} E(Plane\ stress) \\ \frac{E}{1-v^2}(Plane\ strain) \end{cases}$, E is elastic modulus, and v is Poisson's ratio.

When the K-dominant zone is larger than the boundary of the inelastic zone at the crack tip (i.e., small-scale yielding), $K_I(t)$ is calculated through equation conversion.

To explore the feasibility of using dynamic fracture toughness to characterize the crack initiation behavior of high-strength ship hull structural steel joints under explosive loading, explosion numerical simulations were conducted using the explicit dynamics software Ls-dyna. The crack initiation mechanism was explored by solving the J-integral value and converting it into the K value.

Fracture analysis requires a very small mesh, which is very time-consuming. To improve computational efficiency, the 3D explosion simulation model was simplified into a plane strain model, including the air domain, TNT, the butt joint test plate, and the backup plate. A 0.1 mm mesh was divided at the heat-affected zone and weld center of the butt-welded test plate to obtain more detailed stress results. The fluid–structure coupling algorithm (arbitrary Lagrange–Euler algorithm) was used. The finite element model and local mesh are shown in Figure 16.

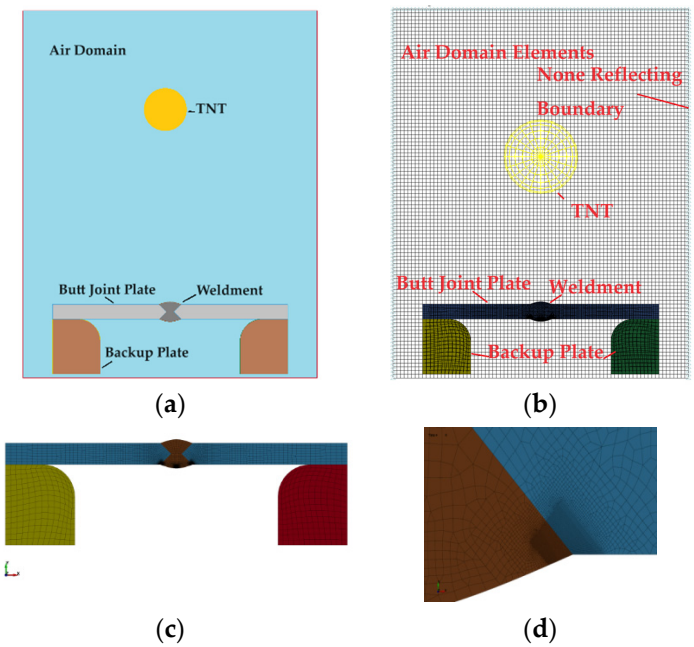

Figure 16. FEM for crack initiation study: (**a**) geometry model; (**b**) element model; (**c**) butt joint model; (**d**) local grid detail diagram of butt joint model.

Under explosive loading, the cumulative damage contour map of the butt joint plate was plotted, which is shown in Figure 17. According to the evolution process of the damage, the crack first initiates at the weld toe on the left side of the butt-welded test plate and continues to propagate along the fusion line. Then, the crack initiates at the weld toe on the right side, while the plastic damage generated in the center of the weld is minimal, and no fracture failure occurs.

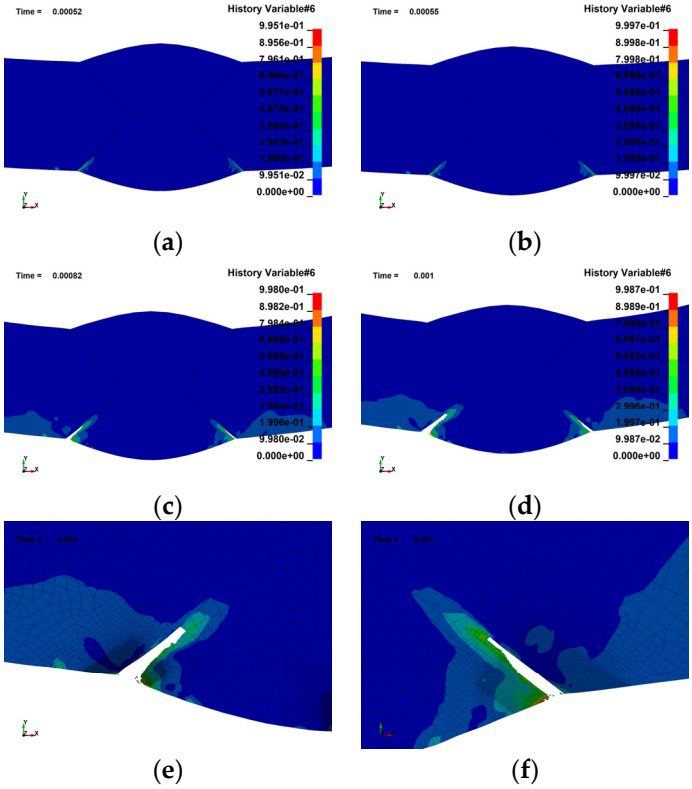

Figure 17. Simulation results of crack initiation: (**a**–**d**) cumulative damage contour plot at different times; (**e**,**f**) partial enlarged detail at weld toes.

Figure 18 shows the cumulative damage time curves extracted sequentially for each element along the right fusion line. As seen from the figure, the cumulative damage of each element gradually reaches 1, and failure occurs toward the plate thickness direction along the fusion line, which is consistent with the crack propagation path in the explosive tests. Among them, the element at the right weld toe begins to fail at 0.64 ms, indicating the dynamic crack initiation of the structure.

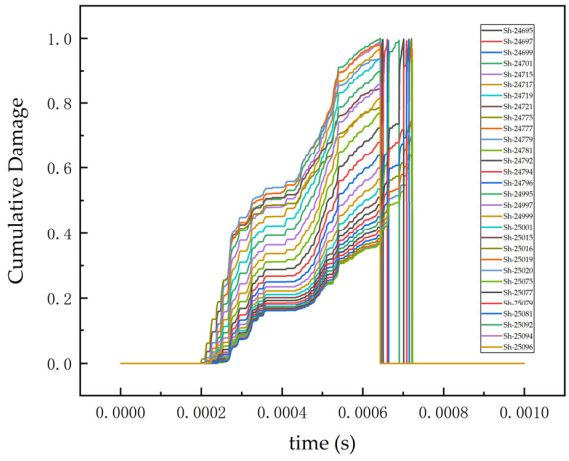

Figure 18. Fusion line elements failure history curve.

The time curves of dynamic fracture intensity factors $K_I(t)$ and dynamic stress intensity factor rate $\dot{K}_{Id}$ for the fusion line element (namely the right weld toe element) and the weld metal element (namely the weld center element) are shown in Figures 19 and 20.

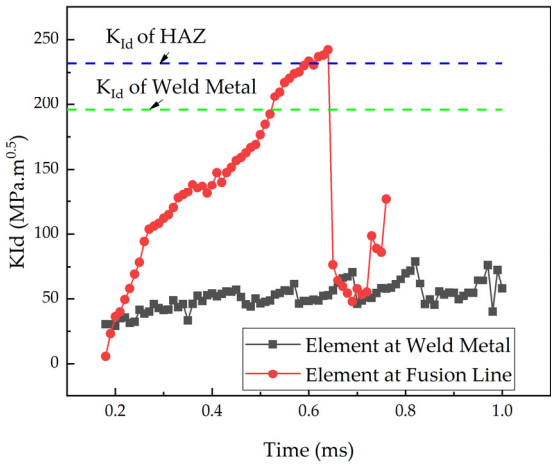

Figure 19. Stress intensity factor history curve.

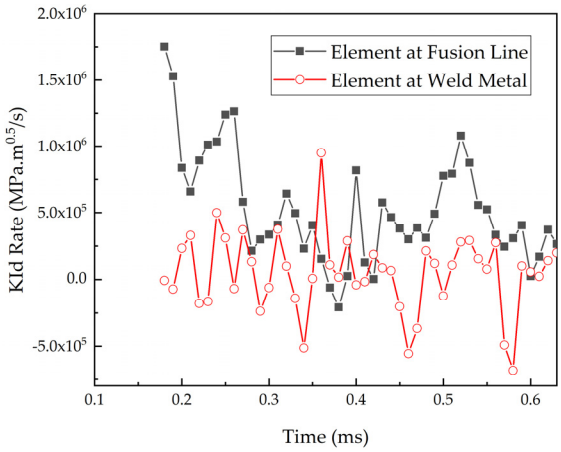

Figure 20. Stress intensity factor rate history curve.

As shown in Figure 19, the dynamic stress intensity factor continuously increases as the explosive load is applied, but it is significantly higher at the fusion line than at the center of the weld. When the dynamic stress intensity factor at the weld toe reaches 240 MPa·m$^{0.5}$, which exceeds the measured dynamic fracture toughness of the heat-affected zone (232 MPa·m$^{0.5}$), fracture failure occurs. However, the dynamic stress intensity factor at the center of the weld remains below the material's dynamic fracture toughness of 196 MPa·m$^{0.5}$, preventing crack failure, consistent with the experimental results. Figure 20 shows that the rate of the dynamic stress intensity factor at the weld toe initially reaches 15×10^5 MPa·m$^{0.5}$/s and then fluctuates and decreases. The rate of the dynamic stress intensity factor at the center of the weld is slightly lower than that at the weld toe.

Obviously, dynamic fracture toughness can effectively predict crack initiation in butt joints under explosive loads.

4.2. Discussion on Dynamic Crack Propagation

Dynamic fracture differs from quasi-static fracture in that it involves stress waves. These stress waves originate from the stress state at the tip of a fracturing crack. If the intensity of the stress wave is high enough, it can also cause crack branching. Since the propagation of fractures is determined by the stress field in the vicinity of the crack wave-

front, it is necessary to understand the relationship between any dynamically propagating crack and the local stress field.

The dynamic crack initiation characteristics of the weld toe under explosive loading in plane strain conditions were obtained, as mentioned above. After crack initiation, the crack will continue to propagate, and during this process, the crack has a complex correlation with stress waves. The maximum principal stress of the crack tip element at different times is shown in Figure 21. As seen in Figure 21, the direction of the maximum principal stress is roughly perpendicular to the crack propagation direction, indicating that the maximum principal stress drives the development of the crack. We can also observe that the crack propagates along the fusion line after initiation, which is consistent with the experimental results.

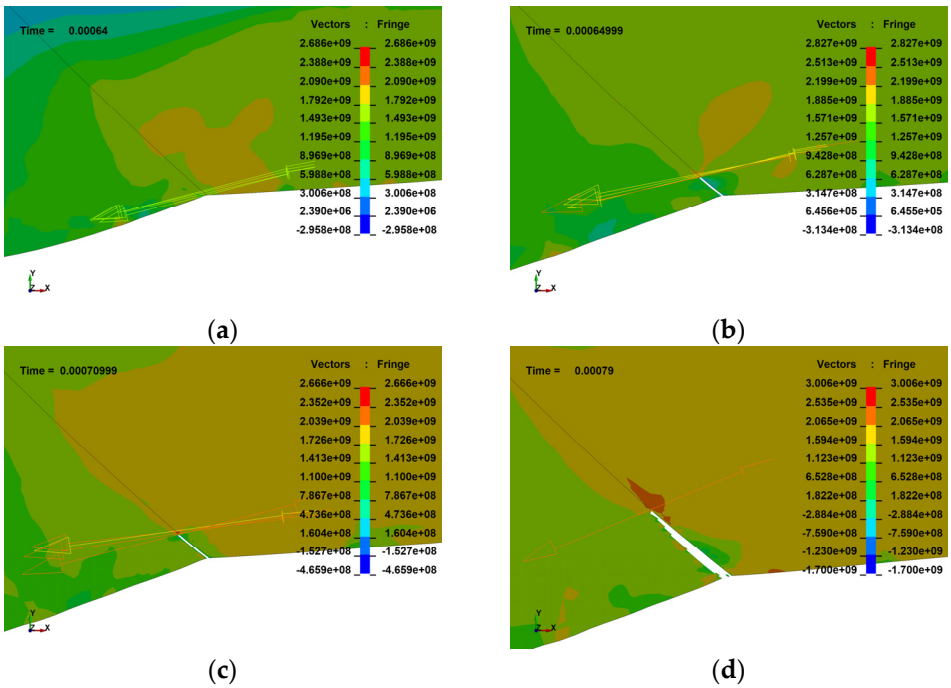

Figure 21. The direction of maximum principal stress on the crack tip: (**a**–**d**) maximum principal stress at different times.

The crack length-time curve as it propagates along the fusion line toward the thickness direction is shown in Figure 22, and the crack propagation rate is depicted in Figure 23. Figure 24 presents the maximum principal stress information of the non-failing element at the crack tip on the fusion line in the tensile region on the right side of the butt joint. Along the crack propagation direction, the maximum principal stress–time curves of different elements were plotted at crack lengths of 0.3 mm (element 9455), 2.25 mm (element 9681), and 3.3 mm (element 8530), as shown in Figure 25.

From the crack length–time curve (Figure 22), it can be observed that the crack propagates intermittently. The crack initiates at 640 μs, and the crack length increases very little between 650 and 710 μs, indicating almost no crack propagation during this period. Then, the crack length rapidly increases again but almost stops propagating between 730 and 760 μs. The crack then resumes propagating at 760 μs. As seen in Figure 23, the crack propagation speed can reach 2000 m/s.

From Figure 24, it can be observed that the maximum principal stress of element sh-9455 near the crack tip exhibits significant fluctuations, with a time interval between peaks of approximately 120 μs. For ship hull structural steel, the stress wave propagation speed ranges from 5000 m/s to 6000 m/s. Considering the butt joint test plate's width of 640 mm, and that the element sh-9455 is located near the center of the plate, the time required for a stress wave to travel from this element to the boundary and reflect back,

covering a distance of approximately 640 mm, is approximately 100–130 μs, which aligns with the peak interval obtained from the simulation.

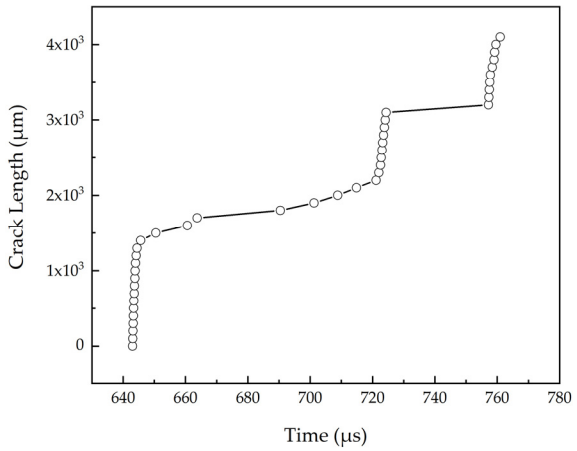

Figure 22. Crack length history curve.

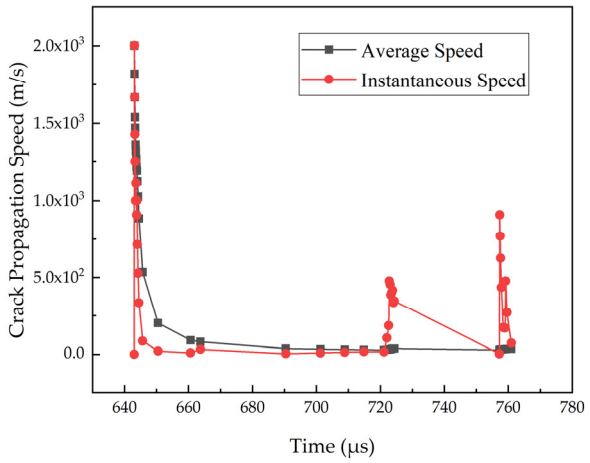

Figure 23. Crack propagation rate history curve.

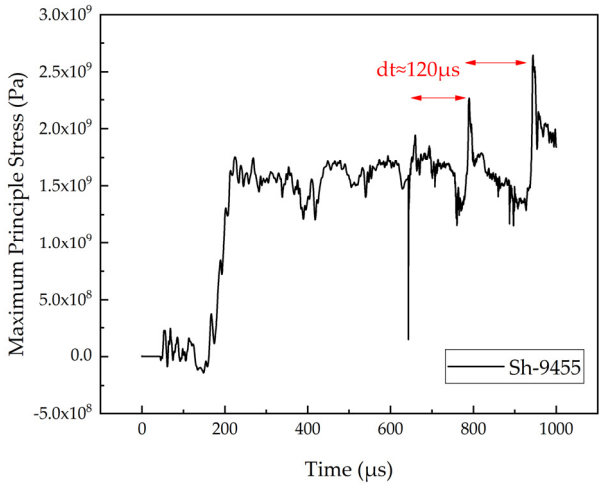

Figure 24. History curve of the maximum principal stress on the crack tip.

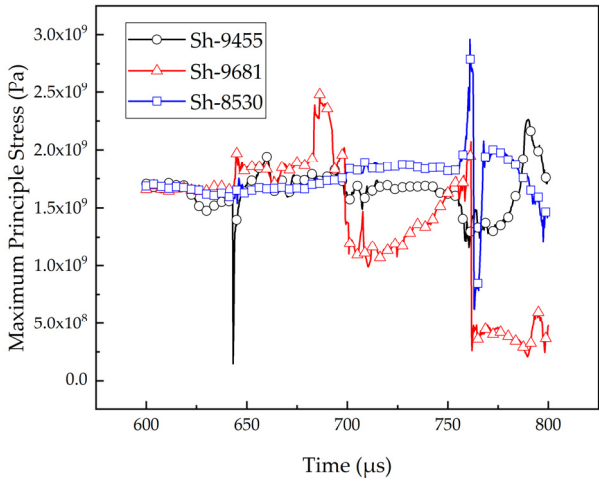

Figure 25. Maximum principal stress on the crack tip.

Based on the further analysis of the crack length–time curve in Figure 22 and the crack propagation rate–time curve in Figures 23 and 25, it can be observed that there are three rapid crack propagation stages during the process, which correspond to three steep rises in the crack length or instantaneous speed in the figures. In Figure 25, the maximum principal stress of element Sh9455 first increases and then decreases sharply at 640 μs, corresponding to the first steep rise in the crack length graph, which indicates the initial crack propagation. The maximum principal stress of element sh-9681 increases rapidly and then decreases sharply at 700 μs, corresponding to the second steep rise in the crack length graph. Similarly, the maximum principal stress of element sh-8530 shows a rapid increase and subsequent sharp decrease at 760 μs, corresponding to the third steep rise in the crack length graph.

This indicates that the crack tip rapidly propagates under the influence of stress waves, and almost no propagation occurs in the absence of stress waves.

5. Conclusions

Through dynamic fracture toughness tests using instrumented impact tests, as well as explosion tests and simulation of butt joints, the following conclusions were obtained:

(1) The dynamic fracture toughness of high-strength ship hull structural steel and welded joints was determined through instrumented Charpy impact tests using specimens with prefabricated cracks. The results show that the dynamic fracture toughness of the base metal is the highest, which reaches 265 MPa·m$^{0.5}$, while the weld metal has the lowest value 196 MPa·m$^{0.5}$. This indicates that welded joints in naval ship hull structures are weak areas; therefore, special attention should be paid to welding applications in ship design.

(2) The stress state and strain rate at the crack tip of a Charpy impact specimen are consistent with that of a welded joint under explosive loads. The strain rate of the weld joint under explosive load is around 1500/s, and the stress triaxiality at the weld toe is about 1.5–2.0, indicating that the weld undergoes tensile failure.

(3) Combining explosion tests and simulation, the dynamic fracture toughness can be used to predict the crack initiation and propagation characteristics of the welded structure. When the local dynamic stress intensity factor of the structure exceeds the material's dynamic fracture toughness, the crack begins to propagate.

(4) The maximum principal stress at the crack tip is perpendicular to the crack surface, and the superposition of stress waves will promote crack propagation. The crack propagation speed can reach 2000 m/s, resulting in instant rupture of the naval ship. Ship designers should avoid fracture as much as possible.

(5) Through dynamic fracture toughness tests, the dynamic property of ship hull steel can be preliminarily evaluated, which is of great significance for material research and

development. Combining explosion tests and simulation, we can predict the failure of welded joints, further improve the joint design, and enhance the anti-explosion level of naval ships. The method proposed in this article can also be applied to armored vehicles, welded protective structures, and other fields.

Author Contributions: P.D., study design and manuscript writing; X.G., conceptualization; L.S., methodology; J.N., supervision; Y.Z., visualization; L.X., validation. All authors have read and agreed to the published version of the manuscript.

Funding: This research received no external funding.

Institutional Review Board Statement: Not applicable.

Informed Consent Statement: Not applicable.

Data Availability Statement: Data are contained within the article.

Conflicts of Interest: The authors declare no conflicts of interest.

References

1. Wang, Y.; Cui, L.; Du, J.; Du, Z. Developments and applications of domestic shock dynamics analysis on naval vessels underwater explosion. *CCTAM* **2009**. Available online: http://172.17.2.25:8088/D/Conference_7204927.aspx (accessed on 8 May 2024).
2. Du, J.; Du, Z.; Li, Y.; Kong, X. The Progress of Naval Ship Explosion Protection Technology. *ACTA Armamentraii* **2015**, *36* (Suppl. 1), 391–400.
3. Li, Y.; Zhang, L.; Du, Z.; Zhou, X.; Xiao, D.; Ren, X.; Fang, D. Failure Mechanism and Anti-Damage Design of Ship Bulkhead under Internal Blast. *Shipbuild. China* **2019**, *60*, 27–34.
4. Ding, P.; Cheng, Y.; Yu, J.; Gong, X.; Wang, R. Experimental Research and Numerical Simulation of Corrugated Sandwich Panel under Explosion Load. *Shipbuild. China* **2021**, *62*, 51–64.
5. Ding, P.; Cheng, Y.; He, L. Experimental measurement and numerical simulation of residual stress on butt welding steel plates. *Dev. Appl. Mater.* **2023**, *38*, 9–16.
6. Hou, H.; Zhu, X.; Mei, Z. Study on the blast load and failure mode of ship structure subject to internal explosion. *Explos. Shock Waves* **2007**, *27*, 151–158.
7. Chuan, P.; Xin, Y.; Han, Z.; Zhen, C.; Ding, X.; Chang, Z.; Bing, X. Numerical Study on Crack Propagation under Explosive Loads. *Acta Mech.Sin.* **2022**, *38*, 421376. [CrossRef]
8. Cheng, S.; Ye, Y.; Zeng, Y.; Gao, R. Failure law of surrounding rock under underground explosion based on a new damage-virtual tensile crack model. *Explos. Shock Waves* **2022**, *42*, 137–149. [CrossRef]
9. Li, Q.; Yang, R.; Li, J.; Qiao, C.; Zhao, Y.; Ma, Y. Experimental Study on Propagation of Dynamic Cracks under Blasting Loading. *Chin. J. Rock Mech. Eng.* **2005**, *24*, 2912–2916. [CrossRef]
10. Yang, R.; Xu, P.; Chen, C. Experimental Study on the Interaction between Explosion Stress Wave and Crack. *Explos. Shock. Wave* **2019**, *39*, 27–37. [CrossRef]
11. Wan, D.; Zhu, Z.; Liu, R.; Liu, B. Effect of two parallel cracks on main propagating cracks under blasting. *Explos. Shock. Waves* **2019**, *39*, 93–104. [CrossRef]
12. Zou, G.; Shen, X.; Wu, L.; Yang, L. Numerical Simulation of Fracture of CT Specimen Loaded by Improved Hopkinson Bar. *J. Harbin Inst. Technol.* **2016**, *48*, 142–147. [CrossRef]
13. Wu, Y.; Li, P.; Xu, Z.; Li, Y. Dynamic Fracture Initiation Toughness Computation of Crack in Pipe Welding Field Under Impact Loading. *At. Energy Sci. Technol.* **2008**, *42*, 661–663.
14. Pan, J. Dynamic Fracture Behavior of Pressure Vessel Materials under Impact Loads. Ph.D. Thesis, University of Science and Technology of China, Hefei, China, 2013.
15. Wang, J. Numerical Simulation and Experimental of Dynamic Fracture Toughness of Metal Materials under High Strain Rate Load. Ph.D. Thesis, Chongqing University of Technology, Chongqing, China, 2019.
16. Yi, H. Study on Dynamic Fracture Toughness of X80 Pipeline Steel Based on CVN Method. Ph.D. Thesis, China University of Petroleum, Beijing, China, 2019.
17. Li, G.; Shi, D.; Wang, L.; Kun, Z. Measurement technology of underwater explosion load: A review. *Ocean Eng.* **2022**, *254*, 111383. [CrossRef]
18. Chen, Y.; Sun, Y.; Wang, C. Damage Characteristics of Ship's Double Bottom Structure Subjected to Underwater Explosion. *Acta Armamentarii* **2023**, *44*, 670–681. [CrossRef]
19. Shen, C.; Zhang, L.; Zhou, Z.; Liu, J. Mechanism of Dynamic Responses of Grillage Structures under Loads of Close-in and Contact Underwater Explosions. *Acta Armamentarii* **2023**, *44*, 1050–1061. [CrossRef]
20. Shi, S.; Wang, R.; Tang, J.; Gun, Y.; Yuan, J.; Chen, Y. Failure mechanism and dynamic response of a composite lattice structure under intense explosion loadings. *Explos. Shock Waves* **2023**, *43*, 102–116. [CrossRef]

21. Gao, P.; Yan, M.; Zhang, Q. Research on scaling law of boundary tearing damage of stiffened plates for ship subjected to underwater explosion load. *J. Vib. Shock* **2024**, *43*, 38–44, 114. [CrossRef]
22. Rossoll, A.; Berdin, C.; Prioul, C. Determination of the Fracture Toughness of a Low Alloy Steel by the Instrumented Charpy Impact Test. *Int. J. Fract.* **2002**, *115*, 205–226. [CrossRef]
23. ESIS. Proposed standard methods for instrumented pre-cracked Charpy impact testing of steels. *Draft* **1996**, *10*, TC5.
24. Schindler, H.J. Estimation of the dynamic J-R curve from a single impact bending test. In *Mechanisms and Mechanics of Damage and Failure*; Petit, J., De Fouquet, J., Henaff, G., Villechaise, P., Dragon, A., Eds.; European Conference on Fracture-11; EMAS: Poitiers, France, 1996; Volume 3, pp. 2007–2012.
25. *E23:2023*; Standard Methods for Notch Bar Impact Testing of Metallic Materials. ASTM International: West Conshohocken, PA, USA, 2023.
26. Ruiz, C.; Mines, R.A.W. The Hopkinson pressure bar and alternative to the instrumented pendulum for Charpy tests. *Int. J. Fract.* **1985**, *29*, 101–109. [CrossRef]
27. Magudeeswaran, G.; Balasubramanian, V. Dynamic fracture toughness behavior of armor-grade Q&T steel weldments: Effect of weld metal composition and microstructure. *Met. Mater. Int.* **2009**, *15*, 1017–1026. [CrossRef]
28. *MIL-STD-2149A(SH)*; Test Method Standard, Standard Procedures for Explosion Testing Ferrous and Non-Ferrous Metallic Materials and Weldments. Department of Defense: Washington, DC, USA, 2 February 1990. Available online: http://www.everyspec.com (accessed on 8 May 2024).

Disclaimer/Publisher's Note: The statements, opinions and data contained in all publications are solely those of the individual author(s) and contributor(s) and not of MDPI and/or the editor(s). MDPI and/or the editor(s) disclaim responsibility for any injury to people or property resulting from any ideas, methods, instructions or products referred to in the content.